



# Revisiting the Epoch of Cosmic Acceleration

David Dahiya<sup>1</sup> and Deepak Jain<sup>2</sup>

<sup>1</sup> Technische Universität Dresden, D-01069 Dresden, Germany; [davddahiya@gmail.com](mailto:davddahiya@gmail.com)

<sup>2</sup> Deen Dayal Upadhyaya College, University of Delhi, Dwarka, New Delhi, India; [djain@ddu.ac.in](mailto:djain@ddu.ac.in)

Received 2022 December 16; revised 2023 May 30; accepted 2023 June 24; published 2023 July 26

## Abstract

We revisit the epoch of cosmic speed-up characterized by the redshift of transition from a decelerated to an accelerated phase. This redshift is termed the transition redshift ( $z_t$ ). We use the spatially flat and non-flat variants of the most common  $\Lambda$ CDM and XCDM models to put constraints on the transition redshift along with the other model parameters. The data for this analysis come from the recent and updated Pantheon+ supernova (SN) data set and the Hubble parameter measurements obtained from Cosmic Chronometers. We consider both data sets with their respective covariance matrices incorporating all statistical and systematic uncertainties. We observe that using the combined data sets of  $H(z)$  and SNe, the best fit value of transition redshift lies in the range  $0.61 < z_t < 0.79$  for all four dark energy models. Incidentally, we observe a positive curvature for the non-flat models, correlations between several model parameters and a strong degeneracy between the curvature and the equation of state parameter.

*Key words:* (cosmology:) dark energy – (cosmology:) cosmological parameters – cosmology: observations

## 1. Introduction

The 1998 study of very distant supernovae (SNe) provided irrefutable proof that, at present, the universe is undergoing an accelerated expansion (Riess et al. 1998; Perlmutter et al. 1999). Through high-redshift SNe, it was established that the early universe was dominated by non-relativistic matter, which supports a decelerating expansion of the universe. Thus, it was apparent that, at a certain epoch, the expansion of the universe shifted from a decelerating phase to an accelerating one. This epoch is characterized by the transition redshift and denoted by the parameter  $z_t$ . It is suggested that  $z_t$  may be a new fundamental cosmological parameter (along with  $H_0$  and  $q_0$ ) that aids in understanding the evolution of cosmic expansion (Melchiorri et al. 2007; Lima et al. 2012).

In recent years, with the influx of new data, several model-independent and model-dependent approaches have been formulated to constrain the transition redshift and other parameters. The model-independent approach does not make any assumptions about the composition of the universe or the theory of gravitation other than assuming a metric structure. This approach involves parameterizations and reconstructions of different kinematic variables, including the Hubble parameter  $H(z)$ , the deceleration parameter  $q(z)$  and the equation of state parameter  $\omega(z)$  in a model independent way (Seikel et al. 2012; Çamlıbel et al. 2020; Al Mamon 2021). For instance, Rani et al. (2015) used three different parameterizations of the deceleration parameter and a local regression method to extrapolate the Hubble parameter and obtained a  $z_t \in [0.60, 0.98]$  (Rani et al. 2015). Similarly, Jesus et al. (2018)

measured a  $z_t \in [0.806, 0.973]$  using different polynomial parameterizations of the comoving distance  $D_C(z)$ ,  $H(z)$  and  $q(z)$  (Jesus et al. 2018). On the other hand, Jesus et al. (2020) relied on a Gaussian process to reconstruct  $H(z)$  and the luminosity distance,  $D_L(z)$ . They obtained transition redshift as 0.59 and 0.683 for the two reconstructions respectively. For a similar reconstruction of  $H(z)$ , Velasquez-Toribio & Fabris (2022) derived a  $z_t \sim 0.7$  (Velasquez-Toribio & Fabris 2022). Capozziello et al. (2021) measured a  $z_t \in [0.473, 1.183]$  after performing a more recent reconstruction of  $H(z)$  and  $q(z)$  incorporating SNe and Hubble data (Capozziello et al. 2021). More methods and parameterizations for obtaining  $z_t$  can be found in Kumar et al. (2023), Koussour et al. (2023), Muccino et al. (2023), Cunha & Lima (2008), Yu et al. (2018), Capozziello et al. (2014).

On the other hand, the model-dependent approach, though relatively simpler, gives a much deeper intuition about the evolution of the universe and its constituents. Current observations strongly favor a universe dominated by a cosmic fluid (dark energy) with negative pressure and constant energy density. This is the standard  $\Lambda$ CDM model of cosmology which can propel the accelerated expansion of the universe (Carroll 2001). Unfortunately, there are still some inconsistencies that the model fails to address, specifically, the fine-tuning and coincidence problems (Frieman et al. 2008; Basilakos & Lima 2010). Therefore, alternate dark energy models such as the XCDM, phantom, quintessence, generalized Chaplygin gas, modified Chaplygin gas, etc. were considered. For example, Melchiorri et al. (2007) used Markov chain

Monte Carlo (MCMC) methods to constrain the parameters in the  $\Lambda$ CDM and other modified dark energy models. The models iterated through different theoretical assumptions and parameterizations and found a  $z_t \in [0.32, 0.48]$  (Melchiorri et al. 2007). Farooq et al. (2017) applied a likelihood maximization technique on three different spatially flat and non-flat models ( $\Lambda$ CDM, XCDM,  $\phi$ CDM) with Hubble data from baryon acoustic oscillations (BAO) and Cosmic Chronometers (CCs). Using different priors on  $H_0$  they found the value of  $z_t \in [0.68, 0.88]$  (Farooq et al. 2017). For more methods and models one can refer to Velasquez-Toribio & Magnago (2020), Wang & Dai (2006), Farooq & Ratra (2013).

Following a similar line of thought, we apply a model-dependent approach in constraining the transition redshift. In this paper, we use the updated compilation of 32  $H(z)$  data points obtained from CCs and the Pantheon+ SN data set containing 1701 data points for the distance modulus. Further, we have utilized the MCMC technique to constrain the model parameters in the spatially flat and non-flat  $\Lambda$ CDM and XCDM models. *This work improves upon earlier works by including the full covariance matrix for both data sets, which incorporates all statistical and systematic uncertainties.* We use the latest data sets and work with models that directly constrain the transition redshift instead of considering it a derived parameter. Additionally, we plot contours to study the correlations between different model parameters. The paper is organized as follows: In Section 2, we describe the  $\Lambda$ CDM and XCDM models. The data sets used and the associated methodology are addressed in Section 3. The final two sections discuss the results and conclusions of this work respectively.

## 2. Models

In this paper, we have considered four different dark energy models. Using the fact that the second derivative of the scale factor  $\ddot{a} = 0$  at the transition epoch, we can derive a relation between the transition redshift and the relative densities of different components in the universe. Taking advantage of this relation, we can find an equation for the Hubble parameter in terms of  $z_t$ .

### 2.1. $\Lambda$ CDM Model

The acceleration equation in the  $\Lambda$ CDM universe dominated by a constant density dark energy is given by

$$\frac{\ddot{a}}{a} = -\frac{4\pi G}{3} \cdot (\rho_T + 3p_T). \quad (1)$$

$\rho_T$  is the total energy density defined by  $\rho_T = \frac{\rho_{m0}}{a^3} + \rho_\Lambda$  and  $p_T$  is the total pressure density.

Using the equation of state parameter  $\omega = 0$  for the matter and  $\omega = -1$  for dark energy in the acceleration equation

$$\frac{\ddot{a}}{a} = -\frac{4\pi G}{3} [\rho_{m0}(1+z)^3 - 2\rho_\Lambda]. \quad (2)$$

Relying on the definition of the transition redshift with  $\ddot{a} = 0$  and the equivalence of the energy densities to the normalized energy densities, we obtain  $z_t$  as

$$z_t = \left( \frac{2\Omega_{\Lambda 0}}{\Omega_{m0}} \right)^{\frac{1}{3}} - 1. \quad (3)$$

Here  $\Omega$  represents the normalized energy densities. For the flat  $\Lambda$ CDM model, the Hubble parameter is expressed as

$$H(z) = H_0 [\Omega_{m0}(1+z)^3 + \Omega_{\Lambda 0}]^{\frac{1}{2}}. \quad (4)$$

Substituting for  $z_t$  along with  $\Omega_{m0} + \Omega_{\Lambda 0} = 1$ , we obtain

$$H(z, f) = H_0 \left[ \frac{(1+z)^3}{\frac{1}{2}(1+z_t)^3 + 1} + \frac{(1+z_t)^3}{(1+z_t)^3 + 2} \right]^{\frac{1}{2}}. \quad (5)$$

Here,  $f$  indicates the free parameters  $H_0$  and  $z_t$  in the flat  $\Lambda$ CDM model. Similarly for the non-flat  $\Lambda$ CDM model, the Hubble parameter is

$$H(z, f) = H_0 [\Omega_{m0}(1+z)^3 + \Omega_{k0}(1+z)^2 + \Omega_{\Lambda 0}]^{\frac{1}{2}}. \quad (6)$$

Here  $\Omega_{k0}$  is a space curvature density parameter and  $z_t$  for the non-flat  $\Lambda$ CDM model is now expressed as

$$z_t = \left( \frac{2(1 - \Omega_{m0} - \Omega_{k0})}{\Omega_{m0}} \right)^{\frac{1}{3}} - 1. \quad (7)$$

After substituting the value of  $z_t$  and using the  $\Omega_{m0} + \Omega_{\Lambda 0} + \Omega_{k0} = 1$  property, the Hubble parameter in non-flat  $\Lambda$ CDM becomes

$$H(z, f) = H_0 \left[ \frac{(1 - \Omega_{k0})(1+z)^3}{\frac{1}{2}(1+z_t)^3 + 1} + \Omega_{k0}(1+z)^2 + \frac{(1 - \Omega_{k0})(1+z_t)^3}{(1+z_t)^3 + 2} \right]^{\frac{1}{2}}. \quad (8)$$

Here,  $f$  indicates the free parameters  $H_0$ ,  $z_t$  and  $\Omega_{k0}$ .

### 2.2. XCDM Model

In the XCDM model, the dark energy acts as a dynamically evolving fluid. Here, the dark energy fluid pressure  $p_X$  and energy density  $\rho_X$  are related as

$$p_X = \omega_X \rho_X, \quad (9)$$

**Table 1**  
Flat Priors Assumed for the Model and Nuisance Parameters

Parameter	Prior Range
$H_0$	[50.0, 90.0]
$z_t$	[0.05, 1.2]
$\Omega_{k0}$	[-0.7, 0.7]
$\omega_X$	[-3.0, 0]
$\alpha$	[0.05, 0.2]
$\beta$	[2, 4]
$M$	[-19.5, -18.9]

where  $\omega_X$  is the constant equation of state parameter having values less than  $-\frac{1}{3}$ .

Solutions to the fluid equation result in the energy density being written as

$$\rho_X = \rho_{X0} \left( \frac{a_0}{a} \right)^{3(1+\omega_X)}, \quad (10)$$

where the subscript ‘‘0’’ defines the current value of the parameters and thus  $a_0$  is assumed to be unity. Substitution in the acceleration equation gives

$$\frac{\ddot{a}}{a} = -\frac{4\pi G}{3} \left[ \frac{\rho_{m0}}{a^3} + \rho_{X0} \left( \frac{1+3\omega_X}{a^{3(1+\omega_X)}} \right) \right]. \quad (11)$$

For the flat  $\Lambda$ CDM model, the condition  $\ddot{a} = 0$  results in

$$z_t = \left[ \frac{-\Omega_{m0}}{\Omega_{X0}(1+3\omega_X)} \right]^{\frac{1}{3\omega_X}} - 1. \quad (12)$$

Here,  $\Omega_{X0}$  is the normalized dark energy density.

For the flat  $\Lambda$ CDM model, the Hubble parameter equation is

$$H(z, f) = H_0 [\Omega_{m0}(1+z)^3 + \Omega_{X0}(1+z)^{3(1+\omega_X)}]^{\frac{1}{2}}. \quad (13)$$

Substituting for  $z_t$ , along with the condition  $\Omega_{m0} + \Omega_{X0} = 1$ , we get

$$H(z, f) = H_0 \left[ \frac{(1+3\omega_X)(1+z_t)^{3\omega_X}(1+z)^3}{(1+3\omega_X)(1+z_t)^{3\omega_X} - 1} + \frac{(1+z)^{3(1+\omega_X)}}{1 - (1+3\omega_X)(1+z_t)^{3\omega_X}} \right]^{\frac{1}{2}}. \quad (14)$$

Here,  $f$  indicates free parameters  $H_0$ ,  $z_t$  and  $\omega_X$ .

For the non-flat  $\Lambda$ CDM model, the Hubble parameter can be written as

$$H(z, f) = H_0 [\Omega_{m0}(1+z)^3 + \Omega_{k0}(1+z)^2 + \Omega_{X0}(1+z)^{3(1+\omega_X)}]^{\frac{1}{2}}. \quad (15)$$

The transition redshift for this model can be expressed in terms of the cosmological parameters as

$$z_t = \left[ \frac{-\Omega_{m0}}{(1-\Omega_{m0}-\Omega_{k0})(1+3\omega_X)} \right]^{\frac{1}{3\omega_X}} - 1. \quad (16)$$

By using the condition  $\Omega_{m0} + \Omega_{X0} + \Omega_{k0} = 1$  and substituting the value of  $z_t$  in the Hubble parameter equation, we obtain

$$H(z, f) = H_0 \left[ \frac{(1-\Omega_{k0})(1+3\omega_X)(1+z)^3(1+z_t)^{3\omega_X}}{(1+3\omega_X)(1+z_t)^{3\omega_X} - 1} + \Omega_{k0}(1+z)^2 + \frac{(1-\Omega_{k0})(1+z)^{3(1+\omega_X)}}{1 - (1+3\omega_X)(1+z_t)^{3\omega_X}} \right]^{\frac{1}{2}}. \quad (17)$$

Here,  $f$  indicates free parameters  $H_0$ ,  $z_t$ ,  $\Omega_{k0}$  and  $\omega_X$ .

### 3. Methodology and Data

In this work, we use the updated 32 Hubble  $H(z)$  measurements obtained from passively evolving galaxies in the redshift range  $0.07 < z < 1.965$  and the 1701 distance modulus  $\mu(z)$  measurements of SNe type Ia (SNe Ia) in the redshift range  $0.001 < z < 2.3$ . We determine the best fit values of the parameters in different cosmological models by minimizing the combined  $\chi^2$  for the two data sets which is given as

$$\chi_{\text{total}}^2 = \chi_{\text{CC}}^2 + \chi_{\text{SNe}}^2. \quad (18)$$

We use the publicly available EMCEE (Foreman-Mackey et al. 2013) Python package to perform MCMC analysis implementing flat priors with ranges listed in Table 1. The analysis yields the joint posterior probability distribution for the model parameters. The distribution is marginalized over other parameters to provide an estimate for the maximum likelihood along with the  $1\sigma$  and  $2\sigma$  confidence intervals. Finally, we use the CORNER (Foreman-Mackey 2016) package to plot the two-dimensional (2D) confidence contours. The following section describes the observational data sets, statistical methods and associated errors in detail.

#### 3.1. $H(z)$ Data

The Hubble data were obtained from spectroscopic dating of massive, passively evolving, low redshift  $z \sim 2$  galaxies. Presently, these galaxies contain no active star formation regions, with most of their stellar mass formed at  $z > 1$ . Chronometers are important as they measure the Hubble parameter directly without assuming a particular cosmological model. Fundamentally, this technique determines the differential ages of adjacent pairs of galaxies ( $\Delta t$ ), given their differential redshift  $\Delta z$ . The ages of these galaxies are directly correlated to the metallicities of their stellar populations. This can be measured by the amplitude of the 4000 Å break in their absorption spectra (Moresco et al. 2016). Finally, the Hubble

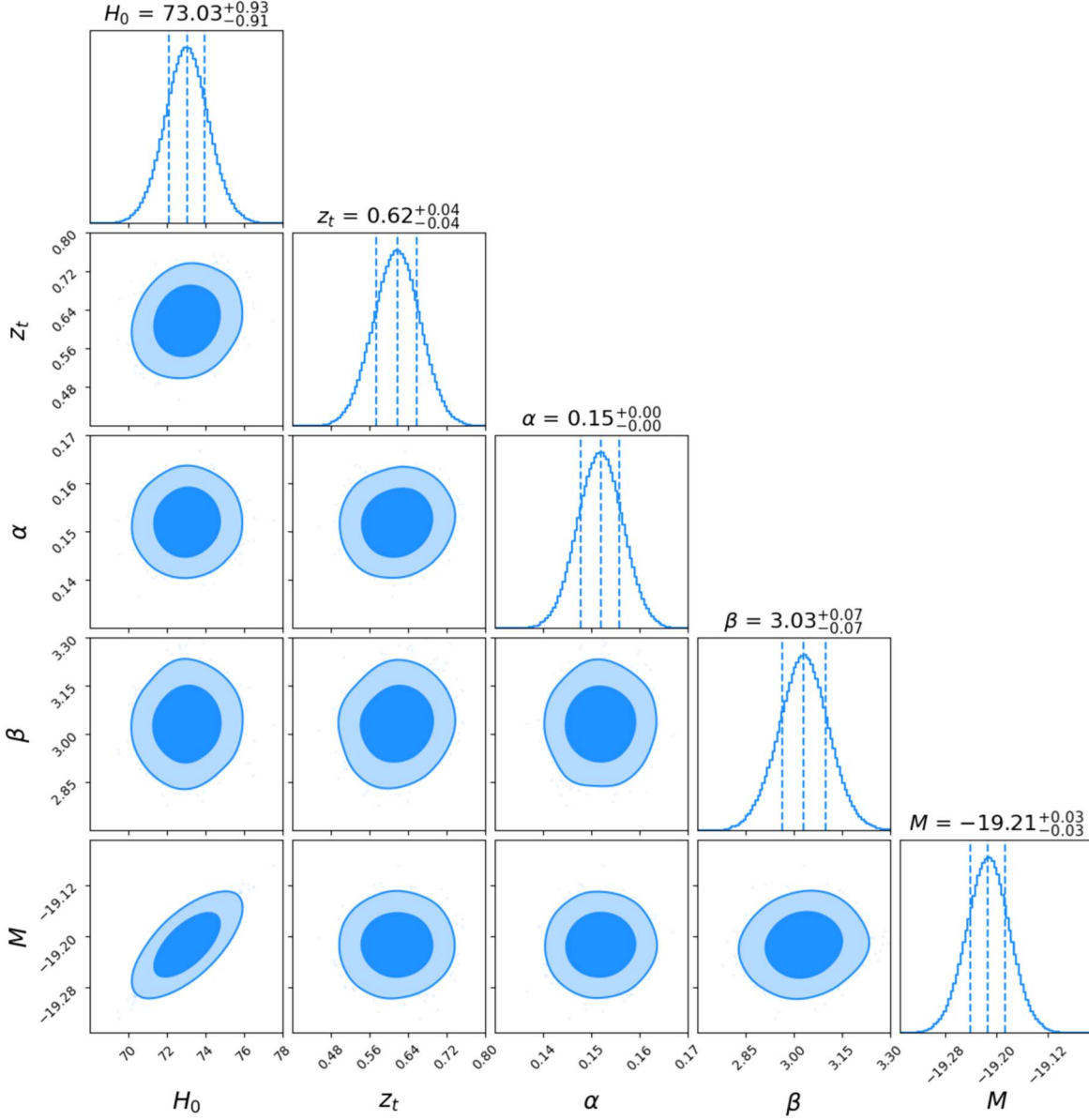


**Figure 1.** Joint confidence contours for the flat  $\Lambda$ CDM model with the CC + SNe data set.

function is written as

$$H(z) = -\frac{1}{1+z} \cdot \frac{dz}{dt}. \quad (19)$$

To account for the complete set of systematic uncertainties, we include the full covariance matrix, represented as the sum of statistical and systematic uncertainties. The matrix is defined as follows

$$\text{Cov}_{ij} = \text{Cov}_{ij}^{\text{stat}} + \text{Cov}_{ij}^{\text{model}}, \quad (20)$$

where the systematic effects arise mainly due to the choice of different models used for estimating ages. The model

covariance includes errors from the initial mass function (IMF), star formation history (SFH), stellar population synthesis (SPS) model and stellar metallicity (SM)

$$\text{Cov}_{ij}^{\text{model}} = \text{Cov}_{ij}^{\text{IMF}} + \text{Cov}_{ij}^{\text{SPS}} + \text{Cov}_{ij}^{\text{SFH}} + \text{Cov}_{ij}^{\text{SM}}. \quad (21)$$

To construct the covariance matrices we use the Mean Percentage Bias ( $\widehat{\eta}^X(z)$ ) table and the following relation from Moresco et al. (2020)

$$\text{Cov}_{ij}^X = \widehat{\eta}^X(z_i) \cdot H(z_i) \cdot \widehat{\eta}^X(z_j) \cdot H(z_j), \quad (22)$$

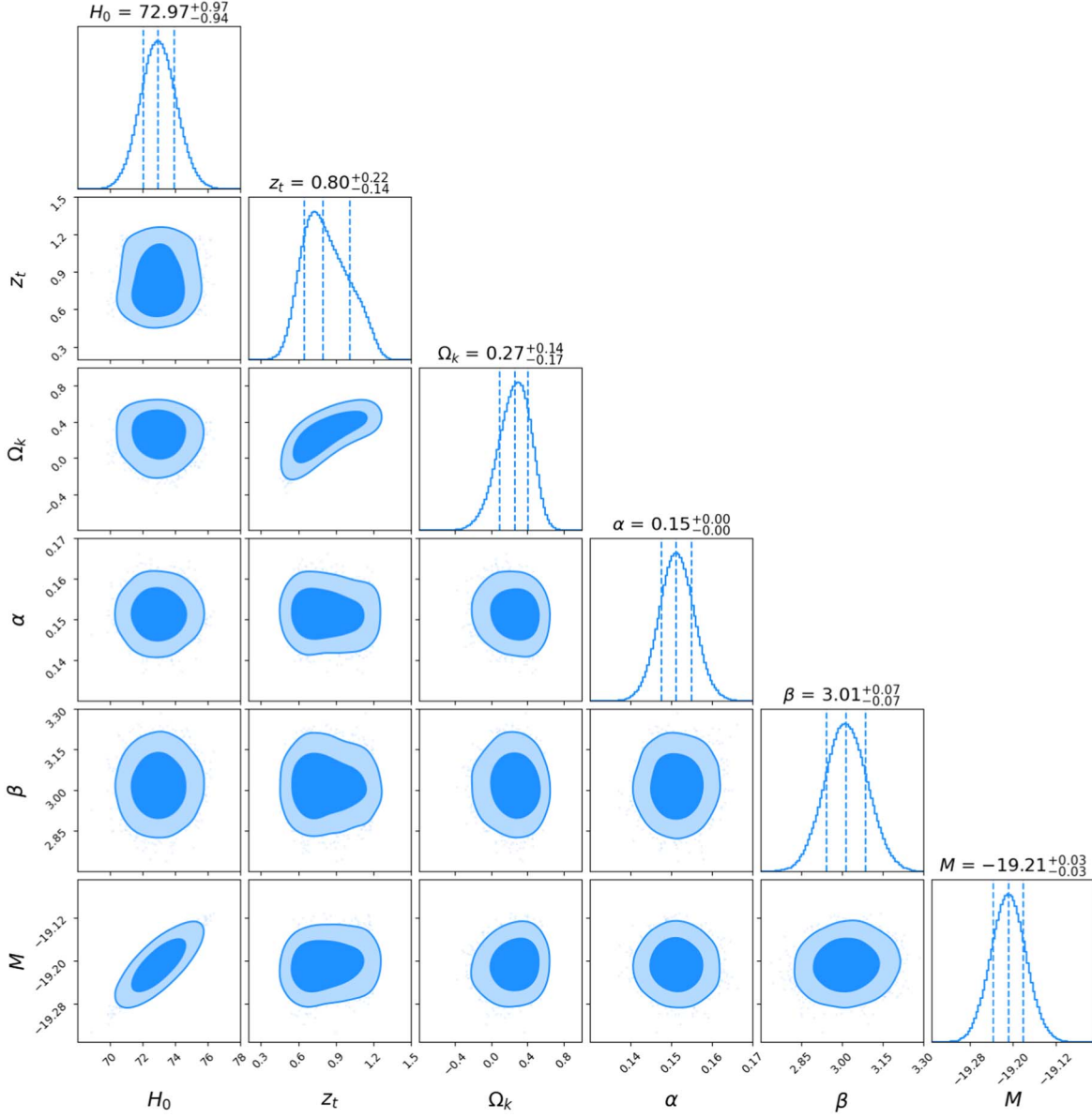


**Figure 2.** Joint confidence contours for the non-flat  $\Lambda$ CDM model with the CC + SNe data set.

where  $X$  represents the contribution from different error components. Using the 32 data points, we construct the  $32 \times 32$  covariance matrix  $\text{Cov}_{\text{stat}+\text{sys}}^{-1}$ . We now calculate  $\chi^2$  and the likelihood as follows

$$-2 \ln(\mathcal{L}) = \chi_{\text{CC}}^2 = \Delta \mathbf{D}^T \cdot \text{Cov}_{\text{stat}+\text{sys}}^{-1} \cdot \Delta \mathbf{D}, \quad (23)$$

where  $\Delta \mathbf{D}$  is the residual vector defined as  $\Delta \mathbf{D}_i = H^{\text{th}}(z_i, \theta) - H^{\text{obs}}(z_i)$ ,  $\Delta \mathbf{D}^T$  represents its transpose and  $\theta$  indicates the model parameters. The  $H^{\text{th}}$  denotes the Hubble parameter

equation for the specific model while  $H^{\text{obs}}$  is the observed value of the Hubble parameter.

### 3.2. Supernova Data

We use the latest Pantheon+ compilation, which analyzes 1701 SN light curves from 1550 distinct SNe in the redshift range of 0.001–2.26. These data include major contributions from CfA1-4, CSP, DES, PS1, SDSS and SNLS. The observed light curves were fitted using a SALT2 model, which returns the best fit value of the parameters  $c$  (color),  $x_1$  (stretch) and  $x_0$

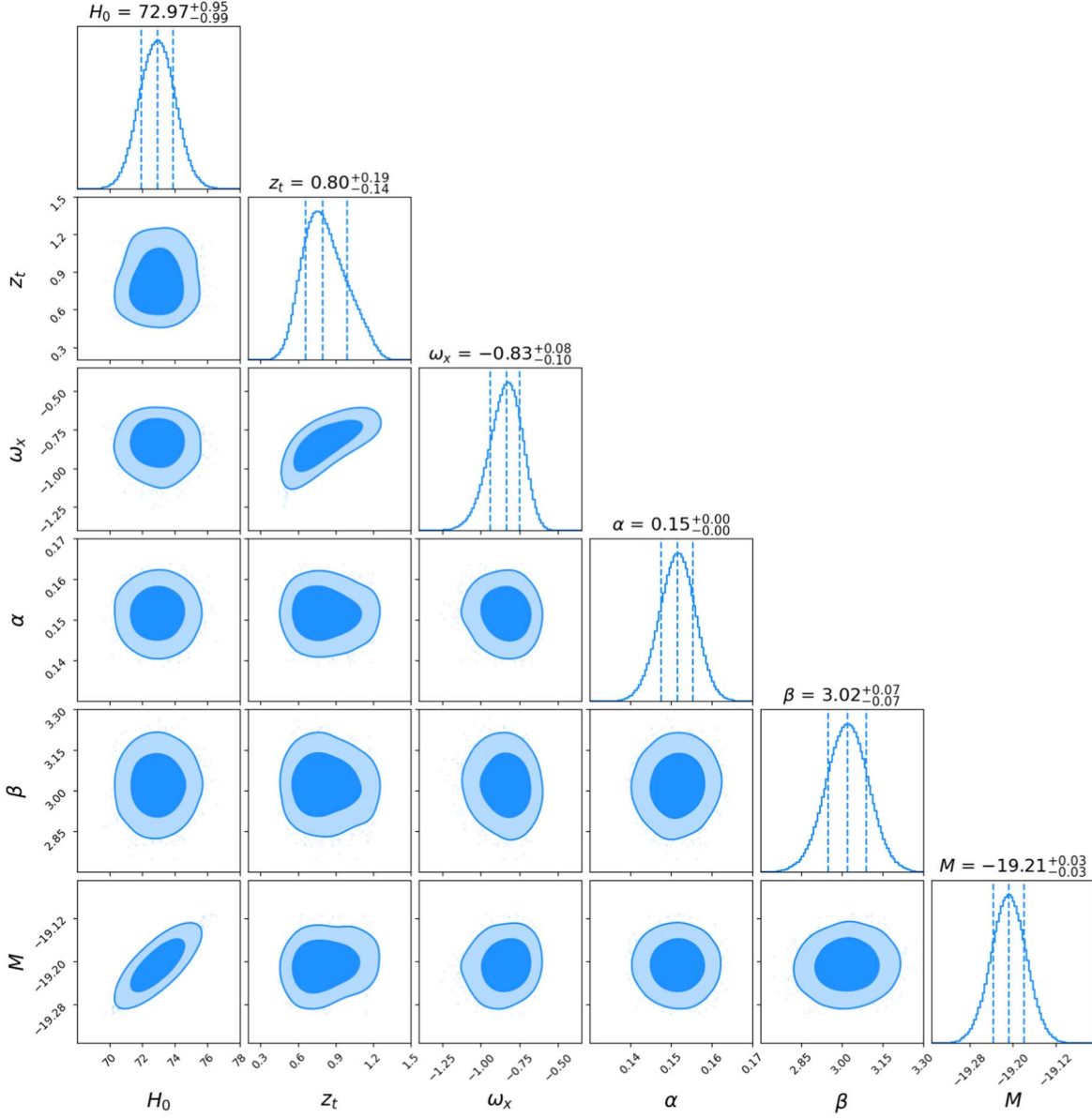


**Figure 3.** Joint confidence contours for the flat XCDM model with the CC + SNe data set.

(overall amplitude) (Scolnic et al. 2022). Given the parameters, we can quantify  $\mu_{\text{obs}}$ , the observed distance modulus, using a linear model expressed as follows

$$\mu_{\text{obs}} = m_B + \alpha x_1 - \beta c - M - \delta_{\mu-\text{bias}}. \quad (24)$$

The nuisance parameters  $\alpha$ ,  $\beta$  and  $M$  are jointly fitted with the cosmological parameters, where  $\alpha$  and  $\beta$  are the coefficients relating stretch and color to luminosity respectively,  $M$  is the absolute magnitude of the SN and  $\delta_{\mu-\text{bias}}$  represents the bias

correction term. Now

$$m_B \equiv -2.5 \log_{10}(x_0). \quad (25)$$

Theoretically the distance modulus is written as

$$\mu_{\text{th}} = 5 \log_{10} \left[ \frac{D_L}{\text{Mpc}} \right] + 25, \quad (26)$$

where  $D_L$ , the luminosity distance, is defined as

$$D_L(z) = (1+z) \cdot c \int_0^z \frac{dz'}{H(z')}. \quad (27)$$

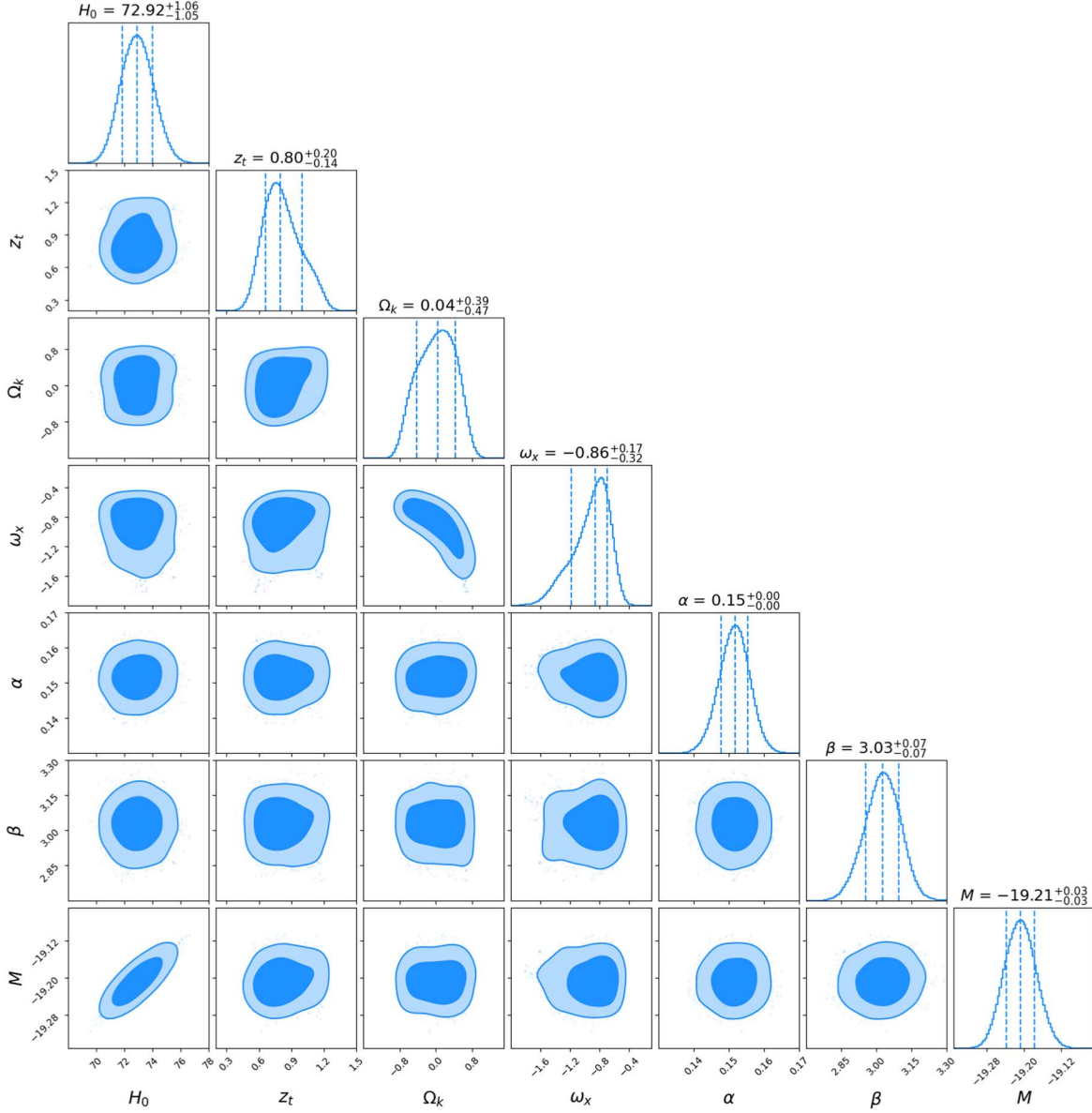


**Figure 4.** Joint confidence contours for the non-flat XCDM model with the CC + SNe data set.

Here  $c$  is the speed of light and  $H(z)$  is the Hubble parameter equation for different models.

Given  $\mu_{\text{obs}}$  and  $\mu_{\text{th}}$ , the residual is defined as

$$\Delta \mathbf{D}_i = \mu_{\text{th}}(z_i, \theta) - \mu_{\text{obs}}(z_i), \quad (28)$$

where  $\theta$  indicates the model parameters. The log-likelihood or  $\chi^2$  relation can now be written as

$$-2 \ln(\mathcal{L}) = \chi_{\text{SNe}}^2 = \Delta \mathbf{D}^T \cdot \text{Cov}_{\text{stat+sys}}^{-1} \cdot \Delta \mathbf{D}. \quad (29)$$

$\text{Cov}_{\text{stat+sys}}^{-1}$  is the  $1701 \times 1701$  square covariance matrix as described in Brout et al. (2022). Because there are 1701 light

curves from 1550 SNe, the statistical covariance matrix includes the distance error ( $\sigma_\mu^2$ ) as the diagonal entry and the measurement noise as the off diagonal terms for duplicate SNe included in multiple surveys. This compilation improves upon earlier works by accounting for a much larger number of systematic uncertainties. These include errors from the measurement of redshift, peculiar velocities and host galaxies; calibration of light curves and the SALT2 model fitting; extinction due to the Milky Way; and simulations of survey modeling, distance modulus uncertainty modeling and intrinsic scatter models.

**Table 2**  
1 $\sigma$  and 2 $\sigma$  Confidence Limit Constraints on the Model Parameters

Model	Data Set	$H_0$	$z_t$	$\Omega_{k0}$	$\omega_X$	$\alpha$	$\beta$	$M$
Flat $\Lambda$ CDM	SNe	73.500 <sup>1.013 2.087</sup> <sub>-0.978 -2.035</sub>	0.587 <sup>0.043 0.096</sup> <sub>-0.043 -0.089</sub>	...	...	0.152 <sup>0.004 0.008</sup> <sub>-0.004 -0.008</sub>	3.024 <sup>0.072 0.149</sup> <sub>-0.073 -0.151</sub>	-19.196 <sup>0.028 0.060</sup> <sub>-0.029 -0.060</sub>
	CC	67.841 <sup>5.392 10.862</sup> <sub>-5.604 -11.337</sub>	0.621 <sup>0.163 0.338</sup> <sub>-0.169 -0.350</sub>	...	...	...	...	...
	SNe + CC	73.034 <sup>0.937 2.069</sup> <sub>-0.899 -1.983</sub>	0.618 <sup>0.040 0.083</sup> <sub>-0.042 -0.086</sub>	...	...	0.152 <sup>0.004 0.008</sup> <sub>-0.004 -0.008</sub>	3.030 <sup>0.068 0.144</sup> <sub>-0.066 -0.147</sub>	-19.213 <sup>0.027 0.057</sup> <sub>-0.027 -0.057</sub>
Non-Flat $\Lambda$ CDM	SNe	73.393 <sup>1.000 2.078</sup> <sub>-0.947 -2.038</sub>	0.723 <sup>0.262 0.433</sup> <sub>-0.160 -0.254</sub>	0.213 <sup>0.179 0.280</sup> <sub>-0.243 -0.525</sub>	...	0.151 <sup>0.004 0.008</sup> <sub>-0.004 -0.008</sub>	3.019 <sup>0.075 0.152</sup> <sub>-0.073 -0.141</sub>	-19.195 <sup>0.029 0.060</sup> <sub>-0.029 -0.061</sub>
	CC	66.538 <sup>5.526 11.782</sup> <sub>-5.409 -10.523</sub>	0.608 <sup>0.220 0.490</sup> <sub>-0.194 -0.452</sub>	0.183 <sup>0.362 0.494</sup> <sub>-0.495 -0.812</sub>	...	...	...	...
	SNe + CC	72.972 <sup>0.979 2.069</sup> <sub>-0.933 -1.958</sub>	0.797 <sup>0.220 0.373</sup> <sub>-0.144 -0.243</sub>	0.266 <sup>0.142 0.233</sup> <sub>-0.171 -0.372</sub>	...	0.151 <sup>0.004 0.008</sup> <sub>-0.004 -0.008</sub>	3.014 <sup>0.075 0.156</sup> <sub>-0.069 -0.145</sub>	-19.208 <sup>0.028 0.059</sup> <sub>-0.028 -0.057</sub>
Flat XCDM	SNe	73.361 <sup>0.980 2.063</sup> <sub>-1.015 -2.074</sub>	0.733 <sup>0.223 0.415</sup> <sub>-0.157 -0.268</sub>	...	-0.866 <sup>0.106 0.171</sup> <sub>-0.138 -0.322</sub>	0.152 <sup>0.004 0.008</sup> <sub>-0.004 -0.008</sub>	3.016 <sup>0.072 0.145</sup> <sub>-0.074 -0.146</sub>	-19.195 <sup>0.027 0.058</sup> <sub>-0.030 -0.062</sub>
	CC	67.321 <sup>8.644 17.790</sup> <sub>-5.979 -10.630</sub>	0.566 <sup>0.241 0.549</sup> <sub>-0.147 -0.395</sub>	...	-1.005 <sup>0.516 0.864</sup> <sub>-0.784 -1.645</sub>	...	...	—
	SNe + CC	72.965 <sup>0.951 1.972</sup> <sub>-0.981 -1.957</sub>	0.799 <sup>0.195 0.365</sup> <sub>-0.140 -0.242</sub>	...	-0.834 <sup>0.083 0.148</sup> <sub>-0.101 -0.218</sub>	0.152 <sup>0.004 0.008</sup> <sub>-0.004 -0.008</sub>	3.020 <sup>0.071 0.149</sup> <sub>-0.072 -0.151</sub>	-19.208 <sup>0.029 0.058</sup> <sub>-0.028 -0.058</sub>
Non-Flat XCDM	SNe	73.244 <sup>1.078 2.190</sup> <sub>-1.033 -2.108</sub>	0.784 <sup>0.221 0.378</sup> <sub>-0.170 -0.307</sub>	0.086 <sup>0.397 0.555</sup> <sub>-0.521 -0.736</sub>	-0.904 <sup>0.199 0.288</sup> <sub>-0.333 -0.619</sub>	0.151 <sup>0.004 0.008</sup> <sub>-0.004 -0.008</sub>	3.016 <sup>0.071 0.139</sup> <sub>-0.073 -0.152</sub>	-19.199 <sup>0.031 0.067</sup> <sub>-0.030 -0.062</sub>
	CC	67.166 <sup>8.008 18.167</sup> <sub>-6.063 -10.802</sub>	0.600 <sup>0.306 0.559</sup> <sub>-0.207 -0.462</sub>	0.293 <sup>0.290 0.392</sup> <sub>-0.498 -0.909</sub>	-1.162 <sup>0.668 1.023</sup> <sub>-1.183 -1.747</sub>	...	...	...
	SNe + CC	72.922 <sup>1.071 2.149</sup> <sub>-1.037 -1.959</sub>	0.798 <sup>0.203 0.368</sup> <sub>-0.135 -0.237</sub>	0.044 <sup>0.389 0.604</sup> <sub>-0.461 -0.698</sub>	-0.863 <sup>0.167 0.254</sup> <sub>-0.313 -0.625</sub>	0.152 <sup>0.004 0.008</sup> <sub>-0.004 -0.007</sub>	3.028 <sup>0.067 0.135</sup> <sub>-0.072 -0.150</sub>	-19.207 <sup>0.029 0.061</sup> <sub>-0.031 -0.058</sub>

**Table 3**

A Summary of the Current Constraint on the Transition Redshift Obtained from Different Works. (KM: Kinematic Models, CF: Cosmographic Functions, GP: Gaussian Process, WFR: Weighted Function Regression)

Method	Model	Data Set	$z_t$	Reference	
Likelihood Maximization	KM: $q(z)$	SNe(SNLS)	0.61	Cunha & Lima (2008)	
	KM: $\omega(z)$	BAO + CMB(WMAP) + SNe(Union)	0.7–1	Magaña et al. (2014)	
	KM: $q(z)$	Age of Galaxies + Strong Lensing + SNe(JLA)	0.6–0.98	Rani et al. (2015)	
	KM: $H(z), D_L(z), q(z)$	CC + SNe(JLA)	0.806–0.973	Jesus et al. (2018)	
	KM: $q(z)$	CC + BAO + SNe(Pantheon) + CMB	0.593–0.792	Al Mamon (2021)	
	$\Lambda$ CDM Model	CC	CC + BAO	0.64	Moresco et al. (2016)
				0.723–0.832	Farooq et al. (2017), Farooq & Ratra (2013)
		CC + BAO + SNe(Pantheon)	0.69	Velasquez-Toribio & Magnago (2020)	
		<b>CC + SNe (Pantheon+)</b>	<b>0.61–0.79</b>	<b>Present Work</b>	
		CF: $H(z)$	CC + BAO + SNe(Pantheon)	0.6857	Koussour et al. (2023)
	CF: $H(z), q(z), j(z)$	CC + BAO + SNe(Union)	0.77–0.86	Capozziello et al. (2014)	
	CF: $a(t)$	BAO + SNe(Union2.1)	0.28–0.63	Muthukrishna & Parkinson (2016)	
	CF: $H(z), q(z)$	SNe (Pantheon) + BAO + GRB	0.739–0.831	Muccino et al. (2023)	
	XCDM Model	CC + BAO	CC + SNe(Pantheon+)	0.684–0.813	Farooq et al. (2017), Farooq & Ratra (2013)
				<b>0.79</b>	<b>Present Work</b>
$\phi$ CDM Model	CC + BAO		0.690–0.885	Farooq et al. (2017), Farooq & Ratra (2013)	
Regression	GP: $H(z), D_L(z)$	CC + SNe(Pantheon)	0.57–0.69	Jesus et al. (2020)	
	GP: $H(z), q(z)$	CC + BAO	0.637–0.71	Velasquez-Toribio & Fabris (2022)	
	GP: $q(z)$	CC + SNe(Pantheon)	0.61	Yang & Gong (2020)	
	GP: $H(z)$	CC + BAO	0.44–0.65	Yu et al. (2018)	
	WFR: $q(z), j(z)$	CC + BAO + SNe(Pantheon + MCT)	0.8	Gómez-Valent (2019)	
	LOESS+SIMEX	Age of Galaxies + Strong Lensing + SNe(JLA)	0.7	Rani et al. (2015)	

#### 4. Results

In this paper, we use the updated available  $H(z)$  and SN data sets along with their full covariance matrices to obtain the constraints on the transition redshift,  $H_0$ , and other model parameters such as  $\omega_X$  and  $\Omega_{k0}$ . Nuisance parameters  $\alpha$ ,  $\beta$  and  $M$  are also jointly fitted to account for any additional bias. The 2D contours and one-dimensional posterior probability distributions for the cosmological parameters are shown in Figures 1–4. The best fit values of the model parameters obtained from different data sets are listed in Table 2.

1. For the  $\Lambda$ CDM model the Hubble parameter  $H_0$  and the transition redshift are tightly constrained. With both the data sets (SNe + CC), the spatially flat model supports an  $H_0 = 73.034_{-0.899}^{0.937}$  and a transition redshift of  $z_t = 0.618_{-0.042}^{0.040}$ , while the non-flat  $\Lambda$ CDM model supports an open geometry ( $\Omega_{k0} = 0.266_{-0.171}^{0.142}$ ) with an  $H_0$  value of  $72.972_{-0.933}^{0.979}$  and a transition redshift of  $0.797_{-0.144}^{0.220}$ .

2. The spatially flat XCDM model suggests a dynamically evolving fluid ( $\omega_X = -0.834_{-0.101}^{0.083}$ ) with an  $H_0 = 72.965_{-0.981}^{0.951}$  and a transition redshift of  $0.799_{-0.140}^{0.195}$ . On the other hand, the non-flat XCDM model also suggests slightly open geometry ( $\Omega_{k0} = 0.044_{-0.461}^{0.389}$ ) with an  $H_0$  value of  $72.922_{-1.037}^{1.071}$ , a transition redshift of  $0.798_{-0.135}^{0.203}$  and an equation of state  $\omega_X = -0.863_{-0.313}^{0.167}$ .
3. The nuisance parameters are consistent across all models with little deviations between the flat and non-flat models. The parameter  $\alpha$  ranges from 0.151 to 0.152,  $\beta$  ranges from 3.014 to 3.030 and  $M$  ranges from  $-19.207$  to  $-19.213$ .

#### 5. Discussion

In this paper, we focus on constraining the transition redshift and build on previous works by using updated data sets with full covariance matrices and additional dark energy models. We express the Hubble parameter equation of dark energy models

in terms of  $z_t$  and, using the MCMC technique, obtain the contours between different model parameters. We observe that, compared to the  $H(z)$  data, the SNe data predict an early time transition (except for the  $\Lambda$ CDM model). Since we observe positive correlations between  $z_t$  and other cosmological parameters ( $\Omega_{k0}$ ,  $\omega_X$ ) from the confidence contours, we can hypothesize that the exception of the  $\Lambda$ CDM model could be a consequence of these correlations. More research is needed to substantiate this claim, nonetheless all models support  $z_t$  in the intermediate redshift range [0.61–0.79]. These results agree with past results obtained from other data sets and methodologies (as mentioned in Table 3). We find negligible difference in the best fit values of SN Ia parameters in each dark energy model studied in this work. Additionally, the constrained nuisance parameters are also consistent with the results obtained earlier in the literature (Betoule et al. 2014; Chen et al. 2022).

The obtained value of current Hubble parameter ( $H_0$ ) differs for the two data sets, further supporting the Hubble tension. The  $H(z)$  data support lower values of  $H_0$  which are in concordance with the Planck cosmic microwave background (CMB) results while the Pantheon+ data set supports a higher value of  $H_0$  which again affirms the results obtained earlier with the SNe data set (Riess et al. 2016; Aghanim et al. 2020).

For all the non-flat models considered in the paper, the non-flat  $\Lambda$ CDM suggests a moderately open geometry ( $\Omega_{k0} > 0$ ) but is still consistent with a spatially flat universe within  $2\sigma$  limits. Similar observations of the curvature parameter were observed earlier by Farooq et al. (2017), Yang & Gong (2021). The non-flat XCDM model, on the other hand, indicates a very mild deviation from a flat universe but has larger error bounds on the curvature density of the universe.

For the dynamical dark energy models, there is mild variation in the equation of state parameter ( $\omega_X \neq -1$ ). Nonetheless, the  $\Lambda$ CDM model ( $\omega_X = -1$ ) can be easily recovered within  $2\sigma$  levels. Our results are consistent with those obtained recently with the Pantheon+ compilation (Brout et al. 2022) and the 2019 DES Compilation (Abbott et al. 2019).

As mentioned above, the non-flat models support an open geometry, although the non-flat  $\Lambda$ CDM model indicates a much stronger positive curvature ( $\Omega_{k0} = 0$  is  $2\sigma$  away) as compared to the XCDM model ( $\Omega_{k0} = 0$  is  $1\sigma$  away). This shows that, when the equation of state is allowed to vary, a flat universe is more statistically probable. Thus, a strong negative correlation exists between the dark energy equation of state and the curvature density which can also be seen in confidence contours for the non-flat XCDM model (Figure 4). This degeneracy is further discussed in Clarkson et al. (2007), Ichikawa et al. (2006) which explore models with different assumptions and discuss the importance of constraining dark energy models in association with the curvature. They also

mention the implications of assuming zero curvature on the equation of state parameter. More information on this degeneracy can be found in Huang et al. (2007), Polarski & Ranquet (2005).

Finally, we observe that when using the combined, updated data sets of  $H(z)$  and SNe along with their full covariance matrices, the best fit value of transition redshift lies in the range  $0.618 < z_t < 0.799$  for all four dark energy models with the standard flat  $\Lambda$ CDM model having the lowest error bars compared to other models. These results are in general agreement with past analyses and the Planck results within the  $2\sigma$  level.

## Acknowledgments

One of the authors (David Dahiya) thanks the Principal, Deen Dayal Upadhyaya College, for providing the facilities where part of the work was done.

## References

- Abbott, T. M. C., Alarcon, A., Allam, S., et al. 2019, *PhRvL*, **122**, 171301  
Aghanim, N., Planck Collaboration, Akrami, Y., et al. 2020, *A&A*, **641**, A6  
Al Mamon, A. 2021, *MPLA*, **36**, 2150049  
Basilakos, S., & Lima, J. A. S. 2010, *PhRvD*, **82**, 023504  
Betoule, M., Kessler, R., Guy, J., et al. 2014, *A&A*, **568**, A22  
Brout, D., Scolnic, D., Popovic, B., et al. 2022, *ApJ*, **938**, 110  
Çamlıbel, A. K., Ibrahim, S., & Feyizoglu, M. A. 2020, *CQGra*, **37**, 235001  
Capozziello, S., Dunsby, P. K. S., & Luongo, O. 2021, *MNRAS*, **509**, 5399  
Capozziello, S., Farooq, O., Luongo, O., & Ratra, B. 2014, *PhRvD*, **90**, 044016  
Carroll, S. M. 2001, *LRR*, **4**, 1  
Chen, R., Scolnic, D., Rozo, E., et al. 2022, *ApJ*, **938**, 62  
Clarkson, C., Cortès, M., & Bassett, B. 2007, *JCAP*, **2007**, 011  
Cunha, J. V., & Lima, J. A. S. 2008, *MNRAS*, **390**, 210  
Farooq, O., Madiyar, F. R., Crandall, S., & Ratra, B. 2017, *ApJ*, **835**, 26  
Farooq, O., & Ratra, B. 2013, *ApJL*, **766**, L7  
Foreman-Mackey, D. 2016, *JOSS*, **1**, 24  
Foreman-Mackey, D., Hogg, D. W., Lang, D., & Goodman, J. 2013, *PASP*, **125**, 306  
Frieman, J. A., Turner, M. S., & Huterer, D. 2008, *ARA&A*, **46**, 385  
Gómez-Valent, A. 2019, *JCAP*, **2019**, 026  
Huang, Z.-Y., Wang, B., & Su, R.-K. 2007, *IJMPA*, **22**, 1819  
Ichikawa, K., Kawasaki, M., Sekiguchi, T., & Takahashi, T. 2006, *JCAP*, **2006**, 005  
Jesus, J., Valentim, R., Escobal, A., & Pereira, S. 2020, *JCAP*, **2004**, 053  
Jesus, J. F., Holanda, R. F. L., & Pereira, S. H. 2018, *JCAP*, **1805**, 073  
Koussour, M., Pacif, S. K. J., Bennai, M., & Sahoo, P. K. 2023, *Fortschritte der Physik*, **71**, 2200172  
Kumar, D., Jain, D., Mahajan, S., Mukherjee, A., & Rana, A. 2023, *Int. J. Mod. Phys. D*, **32**, 2350039  
Lima, J. A. S., Jesus, J. F., Santos, R. C., & Gill, M. S. S. 2012, Is the Transition Redshift a New Cosmological Number?, arXiv:1205.4688  
Magaña, J., Cárdenas, V. H., & Motta, V. 2014, *JCAP*, **1410**, 017  
Melchiorri, A., Pagano, L., & Pandolfi, S. 2007, *PhRvD*, **76**, 041301  
Moresco, M., Jimenez, R., Verde, L., Cimatti, A., & Pozzetti, L. 2020, *ApJ*, **898**, 82  
Moresco, M., Pozzetti, L., Cimatti, A., et al. 2016, *JCAP*, **1605**, 014  
Muccino, M., Luongo, O., & Jain, D. 2023, *MNRAS*, **523**, 4938  
Muthukrishna, D., & Parkinson, D. 2016, *JCAP*, **2016**, 052  
Perlmutter, S., Aldering, G., Goldhaber, G., et al. 1999, *ApJ*, **517**, 565  
Polarski, D., & Ranquet, A. 2005, *PhLB*, **627**, 1  
Rani, N., Jain, D., Mahajan, S., Mukherjee, A., & Pires, N. 2015, *JCAP*, **1512**, 045

Riess, A. G., Macri, L. M., Hoffmann, S. L., et al. 2016, *ApJ*, 826, 56  
Riess, A. G., Filippenko, A. V., Challis, P., et al. 1998, *AJ*, 116, 1009  
Scolnic, D., Brout, D., Carr, A., et al. 2022, *ApJ*, 938, 113  
Seikel, M., Clarkson, C., & Smith, M. 2012, *JCAP*, 2012, 036  
Velasquez-Toribio, A. M., & Fabris, J. C. 2022, *Brazilian J. Phys.*, 52, 115

Velasquez-Toribio, M. A., & Magnago, A. d. R. 2020, arXiv:2001.04645  
Wang, F.-Y., & Dai, Z.-G. 2006, *ChJAA*, 6, 561  
Yang, Y., & Gong, Y. 2020, *JCAP*, 2020, 059  
Yang, Y., & Gong, Y. 2021, *MNRAS*, 504, 3092  
Yu, H., Ratra, B., & Wang, F.-Y. 2018, *ApJ*, 856, 3